Structure
Article

Crystal Structure of RNase T, an Exoribonuclease Involved in tRNA Maturation and End Turnover

Yuhong Zuo,[1,6] Heping Zheng,[2,3,6] Yong Wang,[1] Maksymilian Chruszcz,[2,3] Marcin Cymborowski,[2,3] Tatiana Skarina,[3,4,5] Alexei Savchenko,[3,4,5] Arun Malhotra,[1,*] and Wladek Minor[2,3,*]
[1] Department of Biochemistry and Molecular Biology, University of Miami School of Medicine, Miami, FL 33101, USA
[2] Department of Molecular Physiology and Biological Physics, University of Virginia, Charlottesville, VA 22908, USA
[3] Midwest Center for Structural Genomics
[4] Department of Medicinal Biophysics, University of Toronto, Toronto, ON M5G 2C4, Canada
[5] Ontario Center for Structural Proteomics, Ontario Cancer Institute, Toronto, ON M5G 2C4, Canada
[6] These authors contributed equally to this work.
*Correspondence: malhotra@miami.edu (A.M.), wladek@iwonka.med.virginia.edu (W.M.)
DOI 10.1016/j.str.2007.02.004

SUMMARY

The 3′ processing of most bacterial precursor tRNAs involves exonucleolytic trimming to yield a mature CCA end. This step is carried out by RNase T, a member of the large DEDD family of exonucleases. We report the crystal structures of RNase T from *Escherichia coli* and *Pseudomonas aeruginosa*, which show that this enzyme adopts an opposing dimeric arrangement, with the catalytic DEDD residues from one monomer closely juxtaposed with a large basic patch on the other monomer. This arrangement suggests that RNase T has to be dimeric for substrate specificity, and agrees very well with prior site-directed mutagenesis studies. The dimeric architecture of RNase T is very similar to the arrangement seen in oligoribonuclease, another bacterial DEDD family exoribonuclease. The catalytic residues in these two enzymes are organized very similarly to the catalytic domain of the third DEDD family exoribonuclease in *E. coli*, RNase D, which is monomeric.

INTRODUCTION

All stable RNAs are synthesized as precursors. Maturation of stable RNAs often involves an initial cleavage by endoribonucleases followed by exonucleolytic trimming. In *Escherichia coli*, seven distinct exoribonucleases have been identified (Ezraty et al., 2005; Zuo and Deutscher, 2001). Although many of them, including RNase D, RNase PH, RNase II, and RNase T, contribute to this trimming process, RNase T (RNT) appears to be the most important for the final step of maturation of many stable RNAs (Kelly and Deutscher, 1992; Li and Deutscher, 1995, 1996; Li et al., 1998, 1999). In fact, RNase T is essential for generating the mature 3′ ends of 5S and 23S rRNAs (Li and Deutscher, 1995; Li et al., 1999). RNT is also involved in tRNA end turnover, which consists of the removal and regeneration of the CCA end of tRNA (Deutscher et al., 1985). The latter half of this process involves a universally conserved CCA-adding enzyme, tRNA nucleotidyl transferase. Despite its many important roles, RNT orthologs have been found in only a small group of bacteria, the γ division of *Proteobacteria* (Zuo and Deutscher, 2001).

RNase T is a 3′ to 5′ hydrolytic exoribonuclease (Deutscher and Marlor, 1985). It is one of several *E. coli* proteins belonging to the DEDD superfamily, a large family of 3′–5′ exonucleases which also includes the proofreading domain of many DNA polymerases (Zuo and Deutscher, 2001). Members of this superfamily contain four highly conserved acidic residues distributed in three conserved motifs (Figure 1). In the Klenow fragment, the four acidic residues were shown to bind two divalent metal ions and form the catalytic center (Beese and Steitz, 1991). It is believed that all DEDD family members share a common catalytic mechanism involving two divalent metal ions coordinated by the conserved acidic residues (Steitz and Steitz, 1993). The DEDD family can be divided into two subfamilies, DEDDh and DEDDy, depending on whether a histidine (e.g., in the ε subunit of DNA polymerase III) or a tyrosine residue (e.g., in the Klenow fragment) is conserved in the ExoIII motif (Zuo and Deutscher, 2001). Other than a slight difference in local folding surrounding this residue, the DEDDh and DEDDy exonucleases share a nearly identical fold with the His/Tyr residues occupying an essentially equivalent position. It is believed that a His in DEDDh functions the same way as a Tyr in DEDDy (Breyer and Matthews, 2000; Hamdan et al., 2002). The significance of the difference between a histidine and a tyrosine residue at this position is still unclear. However, it cannot be responsible for the difference between DNases and RNases, as both classes of enzymes are found in the DEDDh and DEDDy groups. RNase T is a member of the DEDDh subgroup. Sequence analysis suggests that RNase T is closely related to DP3E, the proofreading ε subunit of DNA polymerase III, which is another DEDDh member (Koonin and Deutscher, 1993; Zuo and Deutscher, 2001). Interestingly, RNase T also displays

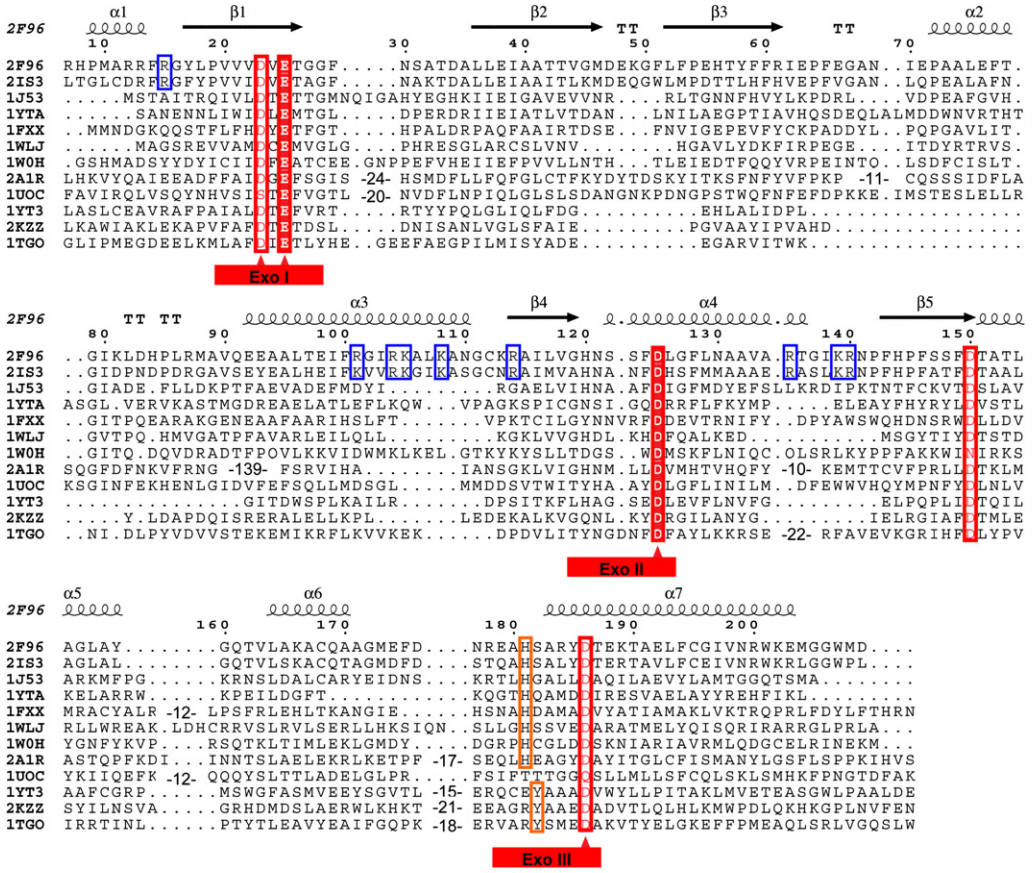

Figure 1. Structure-Based Multiple Alignment of *E. coli* and *P. aeruginosa* RNase T and Related Nucleases

Structures included here are: *E. coli* RNase T (PDB ID code 2IS3); *P. aeruginosa* putative RNase T (PDB ID code 2F96); *E. coli* DNA polymerase III ε subunit (PDB ID code 1J53); *E. coli* oligoribonuclease (PDB ID code 1YTA); *E. coli* exonuclease I (PDB ID code 1FXX); three human 3′–5′ exoribonucleases, PARN (PDB ID code 2A1R), 3′hExo (PDB ID code 1W0H), and ISG20 (PDB ID code 1WLJ); yeast POP2 protein exonuclease domain (PDB ID code 1UOC); *E. coli* RNase D (PDB ID code 1YT3); *E. coli* DNA polymerase I Klenow fragment (PDB ID code 2KZZ); and *T. gorgonarius* DNA polymerase (PDB ID code 1TGO). The last three belong to the DEDDy subgroup, while the others have DEDDh folds. Sequence alignments were initially generated using T-Coffee (http://www.tcoffee.org) (Notredame et al., 2000), followed by some manual adjustment. The three conserved Exo motifs are labeled at the bottom with the DEDD residues marked by red triangles. The NBS basic residues conserved in RNase T orthologs are highlighted using blue rectangles. The numbering at the top is based on the *E. coli* RNase T sequence, with the secondary structure of *P. aeruginosa* RNase T.

strong DNA exonuclease activity (Viswanathan et al., 1998; Zuo and Deutscher, 1999).

Like all DEDD exonucleases, RNase T is a single-strand-specific exonuclease and requires divalent metal ions, such as Mg^{2+} or Mn^{2+}, for its activity (Deutscher and Marlor, 1985; Zuo and Deutscher, 2002c). RNase T is distributive, and displays an unusual base specificity, discriminating against pyrimidines and, particularly, C residues (Zuo and Deutscher, 2002c). Although RNase T appears to bind up to about ten nucleotides, its substrate specificity is defined largely by the last four residues. Another major reason for the specific involvement of RNase T in stable RNA maturation and tRNA end turnover is that RNase T appears to be the only enzyme capable of efficiently removing residues close to a duplex structure without unwinding the double helix. RNase T action slows down significantly as it approaches a duplex; however, it can digest RNA up to the first base pair (Li and Deutscher, 1995) and generate a blunt-ended DNA duplex (Zuo and Deutscher, 1999).

RNase T forms a homodimer in vitro and in vivo, and formation of the dimer is required for it to function (Li et al., 1996a). In addition to confirming that the conserved DEDDh residues are essential for RNase T activity, mutagenesis also identified three short conserved nucleic acid-binding sequence (NBS) segments important for substrate binding (Zuo and Deutscher, 2002a). These three NBS segments are rich in positively charged Arg/Lys residues. Homology modeling using oligoribonuclease, a related DEDD family exoribonuclease as a template, suggested that the NBS segments cluster and form a positively charged surface patch on the face of the RNase T monomer opposite the DEDDh catalytic center (Zuo and Deutscher, 2002b). It was proposed that the two subunits of an RNase T dimer complement each other with substrate binding and catalysis to form fully functional RNase T active sites (Zuo and Deutscher, 2002b).

Table 1. Summary of Data Collection and Refinement Statistics

	P. aeruginosa RNaseT	*E. coli* RNase T	
Data Collection			
Wavelength (Å)	0.9794	0.9786	0.9788
Space group	$P2_1$	I422	
Unit cell dimensions (Å)	a = 49.9, b = 76.6, c = 61.7; 90.0, 93.55, 90.0	a = 213.1, b = 213.1, c = 149.2; 90.0, 90.0, 90.0	
Resolution range (Å)[a]	19.97–2.09 (2.15–2.09)	30.0–3.1 (3.21–3.1)	30.0–3.1 (3.21–3.1)
R_{merge}[b]	0.114 (0.395)	0.092 (0.696)	0.085 (0.845)
$I/\sigma(I)$	17.9 (2.6)	28.9 (2.1)	27.3 (1.4)
Reflections			
Measured	117,164	406,651	396,810
Unique	27,229	31,325	31,269
Completeness (%)	99.5 (96.5)	99.5 (95.1)	98.9 (89.3)
Refinement Statistics			
R factors			
R_{work}	0.158	0.196	
R_{free} (5% data)	0.204	0.231	
Number of atoms			
Protein	3,099	6,039	
Solvent (H_2O/sulfate)	233	65	
Average B factor (Å^2)	28.6	77.4	
Rmsd from ideality			
Bond length (Å)	0.014	0.013	
Bond angle (°)	1.35	1.37	
Ramachandran plot statistics (%)[c]			
Residues in most favored regions	94.0	87.9	
Residues in additional allowed regions	5.7	11.1	
Residues in generously allowed regions	0.3	1.0	
Residues in disallowed regions	0.0	0.0	

[a] Data in parentheses are for the highest-resolution shell.
[b] $R_{merge} = \Sigma(|I_j - \langle I \rangle|)/\Sigma\langle I \rangle$, where I_j is the observed intensity of reflection j and $\langle I \rangle$ is the average intensity of multiple observations. The calculation is performed for merged Bijovet pairs.
[c] Ramachandran plot statistics are taken from PROCHECK (Laskowski et al., 1993).

Here we report two independently solved structures of RNase T, a 2.1 Å resolution RNT structure from *Pseudomonas aeruginosa* (H.Z., M.C., M.C., T.S., A.S., and W.M.), and a 3.1 Å resolution RNT structure from *Escherichia coli* (Y.Z., Y.W., and A.M.). Although RNase T is mostly related to the proofreading ε subunit of DNA polymerase III in sequence, our structures reveal that RNase T adopts an oligoribonuclease-like homodimer architecture with the two monomers arranged in an opposing orientation as proposed previously (Zuo and Deutscher, 2002b). This arrangement juxtaposes the NBS patch from one monomer in the vicinity of the DEDD active center pocket of the other monomer, explaining the requirement of homodimer formation for RNase T activity.

RESULTS

Structure Determination of RNase T

RNase T from *P. aeruginosa* (Midwest Center for Structural Genomics target APC5754) crystallized in the $P2_1$ space group with one RNT dimer in the asymmetric unit. Phasing was performed using single-wavelength anomalous diffraction (SAD), and the structure was refined to a resolution of 2.1 Å with a final R factor of 16% (Table 1); RNase T from *E. coli* crystallized in the I422 space group with four monomers (two dimers) in the asymmetric unit. Phases were obtained using multiwavelength anomalous diffraction (MAD) to 3.1 Å, and the structure was refined to an R factor of 19.6% (Table 1).

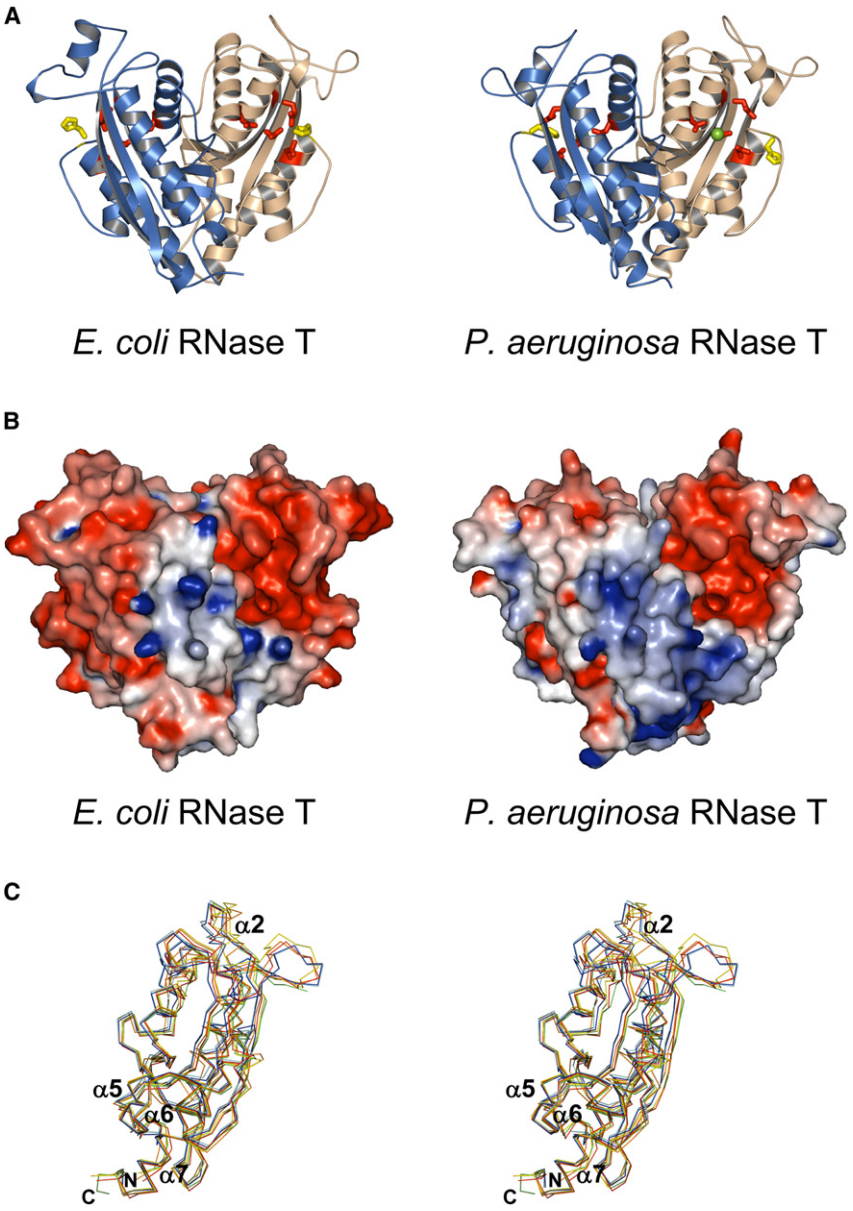

Figure 2. Crystal Structure of *E. coli* and *P. aeruginosa* RNase T

(A) RNase T in a ribbon representation, with the two subunits in each dimer colored differently. Also shown are conserved DEDDh residues (sticks) and bound metal ions (balls).

(B) Molecular surface of RNase T, colored by local electrostatic potential using GRASP (Nicholls et al., 1991). Red color indicates negative potential, blue color indicates positive potential, and both panels use similar scales for electrostatic shading. The larger "blue" patch in the *P. aeruginosa* RNase T reflects a larger number of basic residues in the NBS patch.

(C) Comparison of RNT monomers. The two monomers of *P. aeruginosa* RNase T (PDB ID code 2F96) and the four monomers of *E. coli* RNase T (PDB ID code 2IS3) are superimposed, with only the Cα backbone shown in stereo view. Each monomer is colored differently: cyan, 2F96 chain A; blue, 2F96 chain B; yellow, 2IS3 chain A; green, 2IS3 chain B; red, 2IS3 chain C; and orange, 2IS3 chain D.

RNT forms a compact α/β fold, with the N and C termini coming together at the base of the molecule (Figure 2A). This part of the molecule appears flexible, with the N-terminal ends disordered in both structures (residues 1–18 in *P. aeruginosa*; 1–6 in *E. coli* could not be seen in the electron density). Electron density for several residues at the C-terminal end is missing in both structures. Two internal loop regions in molecule B of *E. coli* RNT (residues 27–36 and 65–84) are invisible in the density map, and appear to be disordered in the crystal. The *E. coli* and *P. aeruginosa* RNT sequences share more than 60% identical residues over the entire sequence. Other than 12 additional residues at the N-terminal end of *P. aeruginosa* RNT, pairwise alignment between *P. aeruginosa* RNT and *E. coli* RNT

shows no gaps (Figure 1). Unless otherwise mentioned, the residue numbers in the entire paper will be based on *E. coli* RNT. The use of the *E. coli* RNT numbering facilitates correlations to earlier biochemical studies, and the residue numbers for *P. aeruginosa* RNT can be readily determined by adding 12. The structures of *P. aeruginosa* RNT and *E. coli* RNT have essentially the same fold, with pairwise root-mean-square deviation (rmsd) between monomer Cα atoms from 0.9 to 1.6 Å, not much higher than pairwise rmsd between monomers within each structure (0.6 Å between *P. aeruginosa* RNT monomers, and 0.6–1.2 Å among *E. coli* RNT monomers). Though several loop regions are flexible, the biggest movement appears to be in the DEDDh-specific α2 region above the DEDD cavity (Figure 2C). All analyses apply to both *P. aeruginosa* and *E. coli* structures unless otherwise specified.

Overall Fold of RNase T

RNase T is a dimer with monomers facing opposite ends (Figure 2). As identified using the DALI server (Holm and Sander, 1996), each monomer has an α/β fold very similar to the catalytic domains of other DEDD family exonucleases, such as the ε subunit of DNA polymerase III (when compared to an *E. coli* RNase T monomer, the Z score is 17.7; Protein Data Bank [PDB] ID code 1J53) (Hamdan et al., 2002), the nuclease domain of exonuclease I (Z score: 16.1; PDB ID code 1FXX) (Breyer and Matthews, 2000), *E. coli* oligoribonuclease (Z score: 13.4; PDB ID code 1YTA) (T.J. Fiedler, Y.Z., and A.M., unpublished data), the nuclease domain of POP2 (Z score: 11.5; PDB ID code 1UOC) (Thore et al., 2003), and several human DEDDh exoribonucleases, 3′hExo (Z score: 16.1; PDB ID code 1W0H) (Cheng and Patel, 2004), ISG20 (Z score: 13.5; PDB ID code 1WLJ) (Horio et al., 2004), and PARN (Z score: 12.5; PDB ID code 2A1R) (Wu et al., 2005). The top Z scores are all against DEDDh proteins. For the DEDDy subfamily, the protein with highest structural similarity to RNT is *Thermococcus* DNA polymerase (PDB ID code 1TGO) (Hopfner et al., 1999), with a Z score of 11.2.

Oligoribonuclease is another homodimeric DEDD exonuclease whose structure has been solved (T.J. Fiedler, Y.Z., and A.M., unpublished data; Gilliland et al., 2002). RNase T and oligoribonuclease share low sequence identity (~15%), yet adopt a very similar homodimeric conformation. The opposing arrangement of two monomers in the RNT homodimer allows putative RNA-binding sites from one monomer to lie very close to the active site of the other monomer (Figure 2B) (Zuo and Deutscher, 2002b). Another DEDD exonuclease, the human poly(A)-specific exoribonuclease PARN, has also been shown to be a homodimer (Wu et al., 2005). However, PARN is a large multidomain protein, and uses a different dimerization interface when compared to RNT (Wu et al., 2005).

RNT Dimeric Interface

Approximately 1300 $Å^2$ are buried for each monomer at the RNase T dimer interface (more than 12% of the total surface area of the monomer). The interface features complementary protuberances and cavities (Figure 3A) that come together to allow RNT to form a very stable dimer, as verified by size-exclusion chromatography at various salt concentrations (Li et al., 1996a). At the center of the highly hydrophobic interface are residues Leu157 and Trp201 from one monomer protruding deep into the other monomer (Figure 3A), contributing about 20% of the buried interface. These two residues are surrounded by conserved hydrophobic residues, including Phe14, Phe149, Leu154, Phe194, Ile197, and Leu204 (Met in *P. aeruginosa* RNT), which form a hydrophobic core at the dimer interface.

Several charged residues also contribute to RNT dimerization. The long aliphatic side chain of Arg15 is part of the hydrophobic dimer interface. Asp150, a residue conserved in almost all DEDD proteins, is also buried at the interface. Replacing Asp150 with alanine leads to a significant loss of RNase T activity (Zuo and Deutscher, 2002a). However, Asp150 appears to be more important for maintaining the local fold rather than contributing to dimerization. A surprising observation is that Arg13 is buried at the interface, forming two hydrogen bonds with the backbone of the other subunit. In a previous study, Arg13 was predicted to be involved in substrate binding, which does not explain the dramatic effect on RNase T activity by an Arg13-to-alanine mutation, as this single mutation led to a large increase in K_m (~15 fold) and a more than 100-fold decrease in V_{max} (Zuo and Deutscher, 2002a). It is evident from the crystal structure that the Arg13-to-alanine mutation likely affects RNase T dimerization. Previous experiments have also shown that mutation of Trp207 makes RNase T temperature sensitive, due to a destabilized dimer conformation (Zuo and Deutscher, 2002a). The crystal structure suggests that Trp207 serves to sequester Arg13 from the bulk solvent. Therefore, the temperature sensitivity of Trp207 mutants might be more of an indirect effect of an exposed Arg13 residue, which would weaken the hydrogen bonds at the dimer interface (Figure 3B).

RNase T Active Center

All DEDD family exonucleases share a common active site geometry, with four acidic side chains that coordinate two divalent metal ions: a site A metal ion coordinated by the three conserved acidic residues from ExoI and ExoIII sequence motifs (Figure 1), and a site B metal ion coordinated by the conserved aspartate residue in ExoI and indirectly by the conserved aspartate in ExoII. Both metal ions interact with the terminal phosphate in the presence of a substrate, and a general catalytic mechanism was proposed involving the two bound metal ions and a conserved tyrosine residue in the ExoIII motif in the case of a DEDDy protein (Beese and Steitz, 1991; Steitz and Steitz, 1993). RNT, a DEDDh member, has all four conserved acidic residues (Asp23 and Glu25 in ExoI, Asp125 in ExoII, and Asp186 in ExoIII), and a conserved histidine in ExoIII (His181). The geometry of the four conserved acidic residues in RNT agrees very well with other DEDD family members. Of the 203 Cα atoms in one *P. aeruginosa* RNT monomer, 140 can be superimposed

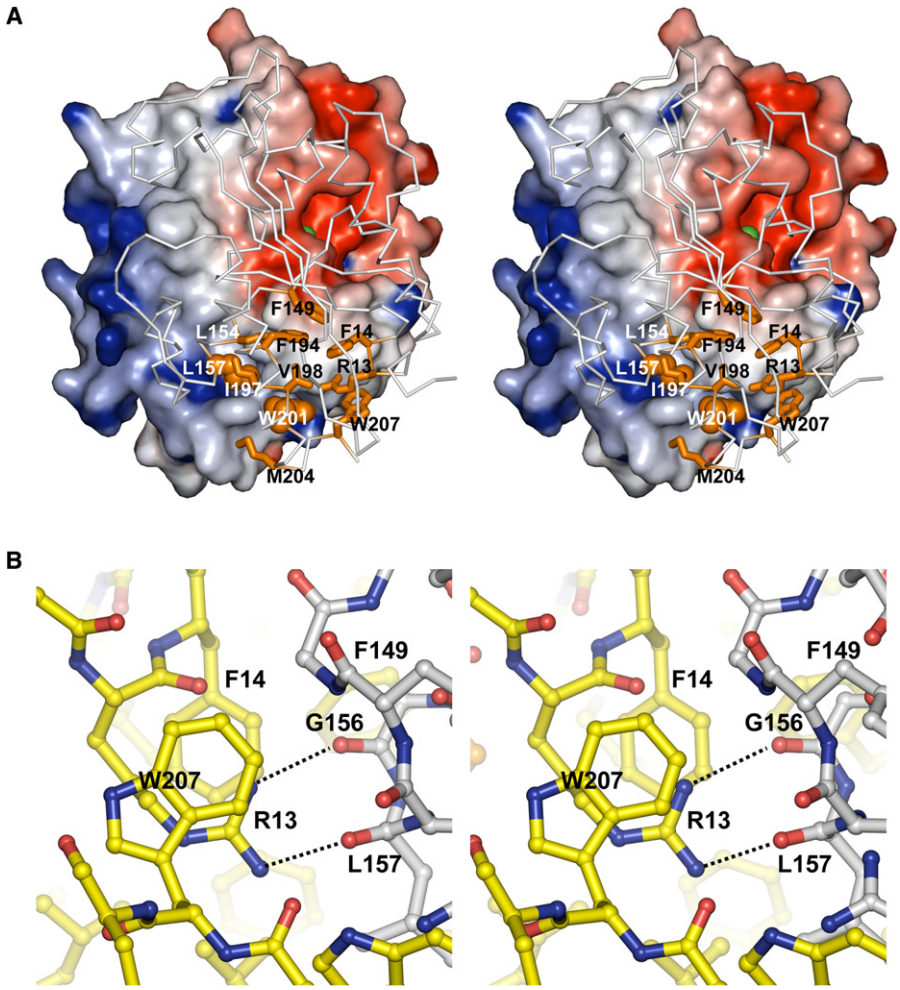

Figure 3. Dimer Interface of RNase T in Stereo View

(A) View of the *P. aeruginosa* RNase T monomer from the dimer interface. One monomer is shown with its molecular surface colored by electrostatic potential as in Figure 2, while the other is shown as a Cα trace (gray) with major interface contributors shown in orange as sticks (Arg13, Phe14, Phe149, Leu154, Phe194, Ile197, Val198, Met204, and Trp207) and balls (Leu157 and Trp201). Both the Leu157 and Trp201 side chains protrude deep into the partner subunit. The metal ion at the active center of the monomer is shown as a green sphere. The residue numbers shown here are that of corresponding *E. coli* RNase T residues. Met204 corresponds to Met216 in *P. aeruginosa* RNase T, and is Leu204 in *E. coli* RNase T.
(B) Details of the *P. aeruginosa* RNase T dimer interface, showing the position of Arg13 and its interactions with Phe14 and Trp207, and the backbone of the partner subunit. The carbon atoms from the two subunits are colored differently.

on *E. coli* exonuclease I Cα traces with an rmsd of 1.60 Å, and 109 can be superimposed on Klenow fragment exonuclease domain Cα traces with an rmsd of 1.58 Å.

No metals were observed in the *E. coli* structure, but a metal ion was observed at the B site of each monomer of the *P. aeruginosa* RNT structure (Figure 4). This B site metal ion has an octahedral coordination typical for a magnesium ion. It is interesting to point out that, in contrast to DEDDy proteins, in which the B site is usually a weaker metal-binding site than the A site (Zuo et al., 2005), DEDDh proteins appear to have stronger B site metal binding in the absence of a substrate. A single metal ion at the B site has also been observed in *E. coli* exonuclease I (Breyer and Matthews, 2000). The absence of a metal ion at the A site of *P. aeruginosa* RNT could also be due to preference for a nonmagnesium metal ion at this site, even though Mg^{2+} by itself supports RNase T activity (Deutscher and Marlor, 1985). In fact, a water molecule (water-164) occupying the A site in *P. aeruginosa* RNT (chain A) might mimic a nonmagnesium metal ion with five potential coordination ligands.

Like other DEDDh proteins, the conserved histidine in the ExoIII motif is part of a highly flexible loop. This conserved histidine residue in DEDDh can occupy a position spatially equivalent to DEDDy tyrosine, and has been proposed to function in a manner similar to the conserved tyrosine residue in DEDDy exonucleases (Breyer and Matthews, 2000; Hamdan et al., 2002). Mutating His181 of *E. coli* RNase T abolishes its exonuclease activity (Zuo and Deutscher, 2002a), suggesting an important

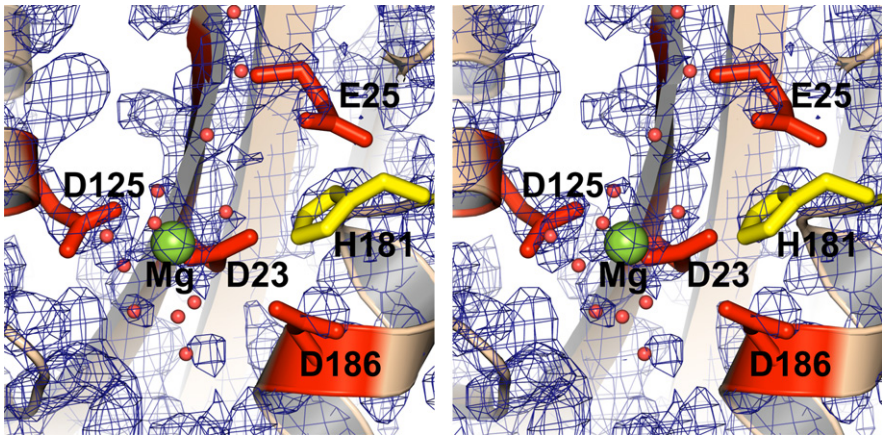

Figure 4. Close-Up of the DEDDh Active Site in *P. aeruginosa* RNase T: Monomer B in Stereo View
The conserved DEDDh residues are shown as sticks (red and yellow). The Mg ion located at the B site is shown as a green sphere. Also shown are a few water molecules (small red spheres) at the active center. The experimental electron-density map after solvent flattening is shown contoured at 2σ.

role of His181 for RNase T catalysis. Interestingly, the two DEDDh histidine residues in each RNT homodimer (two homodimers in the *E. coli* RNT structure and one homodimer in the *P. aeruginosa* RNT structure) adopt different conformations; one is partially directed toward the active center (Figure 4), while the other is facing away from the active center. It is not clear whether this is just a crystal packing artifact, as the histidine directed toward the active center is close to the symmetry-related molecule, or an indication of flexibility in the absence of substrate in the RNT active site.

RNase T Substrate-Binding Site

Both *E. coli* RNT and *P. aeruginosa* RNT are highly negatively charged proteins, with theoretical pIs of 5.2 and 5.0, respectively. However, surface charge distribution is strongly uneven in both proteins (Figure 2B). Nine out of the 18 Arg/Lys residues in *E. coli* RNT (11 out of 23 in *P. aeruginosa* RNT) are found in three short conserved sequence segments, named NBS segments for their likely roles in nucleic acid binding (Zuo and Deutscher, 2002a). The greater number of Arg/Lys residues in *P. aeruginosa* RNT NBS segments is reflected in a larger positive patch (Figure 2B). Except for Arg13, which is buried at the dimer interface, all the NBS basic residues cluster on one side of the monomer surface to form a basic patch, which contains no acidic residues. This basic patch is on a side opposite the DEDD catalytic center cavity. Another basic residue, Lys166, on the edge of the DEDD cavity, extends the basic patch. Mutating the basic residues of the NBS patch, individually or in combination, leads to significantly increased K_m with little effect on the V_{max} of RNase T catalysis (Table 2) (Zuo and Deutscher, 2002a). This is consistent with the suggested role of substrate binding for the NBS patch. The involvement of the NBS patch in substrate binding is also supported by the observation that several SO_4^{2-} anions are bound to this region in the *E. coli* RNase T structure.

DISCUSSION

Requirement of Dimerization for RNase T Action

Prior mutagenesis studies have revealed that the conserved DEDDh residues are essential for RNase T activity, indicating that they likely form the RNase T catalytic center in a manner similar to that found in other DEDD exonucleases (Zuo and Deutscher, 2002a). Our structures confirm

Table 2. Effect of Mutations on *E. coli* RNase T Activity

RNase T Variant	K_m (μM)	Relative Activity[a]
Wild-type RNT	10	100
D23A RNT	23	1.4
E25A RNT	ND	1.3
H120A RNT	ND	5.4
D125A RNT	33	34
H181A RNT	ND	1.4
D186A RNT	25	0.7
D150A RNT	ND	1.4
R13A RNT	~150	0.04
R15A RNT	~100	14
K108A	~150	26
R114A	~120	24
K108A/R114A	~250	6
K139A	~80	35
K108A/K139A	~200	10
K108A/R114A/K139A	>300	2
K108A/R114A/K139A/R140A	>300	0.6

Data are from Zuo and Deutscher (2002a). ND, not determined.
[a] Relative activity was estimated with 20 μg tRNA substrate in a 50 μl reaction (~16 μM).

that RNase T shares the same spatial arrangement of active center residues as seen in other DEDD enzymes. Mutagenesis studies also identified three short sequence segments (NBS segments) important for RNase T substrate binding. These three NBS segments are highly conserved in RNase T orthologs and are rich in positively charged Arg/Lys residues. Like oligoribonuclease, RNase T forms a homodimer and the homodimeric form is required for function (Li et al., 1996a). An oligoribonuclease-like homodimer architecture was thus proposed for RNase T (Zuo and Deutscher, 2002b). According to this homodimer model, the NBS substrate-binding patch and the DEDD center from different subunits are brought together to form fully active sites. Our results confirm this model, and both the *E. coli* and the *P. aeruginosa* RNase T structures show the basic patch from one monomer positioned right next to the DEDD catalytic center cavity of the other monomer in the homodimer (Figure 2B).

Although there is good agreement between the homology model and the crystal structure, there is a surprising observation that the conserved basic residue Arg13 is buried in the otherwise highly hydrophobic dimer interface and forms two hydrogen bonds with the backbone of the other monomer. Arg13 had been predicted to be part of the NBS patch, though its mutation showed a different effect on RNase T activity when compared to mutations of other NBS basic residues (Table 2). In addition to an increased K_m value as seen with other NBS mutations, the Arg13 mutant also displayed a dramatically reduced K_{cat}, which is inconsistent with a residue involved only in substrate binding. The observation that Arg13 is buried at the dimerization interface in the crystal structures suggests that mutating Arg13 might disrupt or significantly weaken the RNase T dimer. The observation of a buried Arg13 also suggests that the temperature sensitivity seen in Trp207 mutants might be more of an indirect effect. In the crystal structure, Trp207 serves to sequester Arg13 from the bulk solvent; Arg13 is sandwiched between Trp207 and Phe14 and participates in cation-π-like interactions with these side chains (Figure 3B). Mutating Trp207 to an Ala or a stop codon would expose Arg13, and thus weaken the hydrogen bonding with the partner subunit. The same could also be true for another C-terminal mutation, Gly206Ser (Li et al., 1996a), which displays an effect consistent with weaker dimerization of RNase T. A Gly206-to-Ser mutation would disrupt the C-terminal folding and thus expose Arg13, even if it does not directly interfere with dimerization.

In contrast to the unexpected involvement of Arg13 in RNT dimerization, the hydrophobic residue Cys168, which was implied in RNT dimerization (Li et al., 1996a), is not at the dimer interface. Instead, Cys168 is part of helix α6 and is buried at the α6/α7 interface. Both α6 and α7 helices are important for shaping the DEDD active center cavity. Mutating Cys168 to less hydrophobic residues (Li et al., 1996a) would likely weaken the anchoring of α6 to α7. It is expected that a displaced α6 would compromise RNase T activity by disrupting the DEDD cavity and the basic patch, as this helix also harbors the conserved basic residue Lys166. It is also possible that a displacement of this helix will interfere with RNT dimerization, as α6 is close to, both in sequence and in space, α5 and the C terminus of α7, which are major contributors to the dimer interface.

Making Sense of RNase T Substrate Binding

RNase T has been shown to be important for the 3′ maturation of many stable RNAs as well as tRNA end turnover in vivo (Deutscher et al., 1985; Kelly and Deutscher, 1992; Li and Deutscher, 1995, 1996; Li et al., 1998, 1999). All RNase T substrates share a common feature: their 5′ and 3′ ends pair with each other to form a stable, double-stranded stem followed by a few unpaired 3′ nucleotides (Li et al., 1998). Later studies with model substrates demonstrated that RNase T is a single-strand-specific exonuclease that can act on both DNA and RNA substrates (Zuo and Deutscher, 1999, 2002c). The important role of RNase T in stable RNA maturation was thus attributed to its unique ability to efficiently remove residues near a stable duplex without substrate unwinding.

Docking studies (data not shown) indicate that RNase T can make favorable interactions with up to 11–12 nucleotides upstream of the 3′ end for a flexible single-stranded substrate. Other than the 3′-terminal 3–4 nucleotides, which are mostly inside the DEDD cavity, contacts are expected between the nucleic acid backbone and the positively charged side chains on the NBS basic patch.

Interactions of duplex substrates with RNase T are likely to be more restricted due to the need for accommodating the helical stem on the NBS and for proper presentation of the 3′ overhang into the DEDD active center. For duplex-containing RNA substrates, such as tRNA or tRNA precursors, a 3′ overhang of five nucleotides or longer appears to be preferred. Due to potential steric hindrance by the complementing 5′-end residues, a substrate with shorter 3′ overhang would either not be able to interact with the NBS patch at the far end or have to disrupt the stacking on the 3′ end (Figure 5A). This explains the impeding effect of a duplex on RNase T activity. In fact, the active center cavity can well accommodate a DNA/RNA duplex with a one-nucleotide 3′ overhang, suitable for generating a blunt-ended duplex (Zuo and Deutscher, 1999). Docking shows that a DNA duplex substrate with a 3′ overhang as short as a single nucleotide should be able to nicely interact with the entire RNase T NBS patch due to its wide major groove; on the other hand, an A-form RNA duplex with a short 3′ overhang is likely to make fewer contacts with the NBS patch due to steric clashes (Figure 5B).

The physiological role of RNase T is also defined by its unusual sequence specificity, discriminating against pyrimidine and, particularly, C residues at the 3′ end. This sequence specificity is defined largely by the last four residues (Zuo and Deutscher, 2002c). A single 3′-terminal C residue can reduce RNase T action by more than 100-fold, and two terminal C residues essentially stop the enzyme. RNase T prefers a substrate with a CCAN, especially CCAA, sequence at the 3′ end (Zuo and Deutscher, 2002c). This makes RNase T well suited for tRNA maturation while preventing overdigestion of the CCA end. All

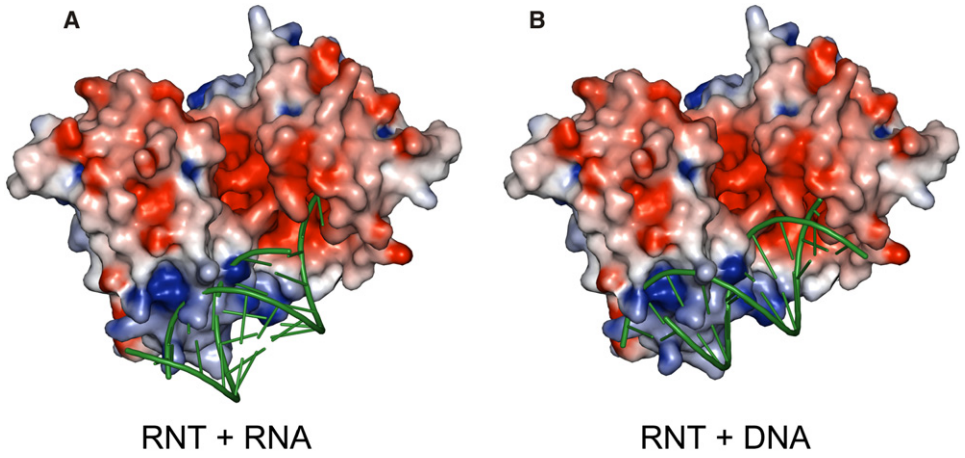

Figure 5. Possible Binding Modes for Duplex-Containing Substrates on *P. aeruginosa* RNase T

(A) Docking of an ideal A-form RNA duplex with a two-nucleotide 3′ overhang. Although the unpaired 3′ overhang is shown stacked here, this region is likely to be distorted for hydrolytic cleavage.

(B) Docking of an ideal B-form DNA helix with a single-nucleotide 3′ overhang. RNase T is shown as a surface potential diagram colored as in Figure 2, and substrates are shown as green ribbons. Only one substrate molecule was docked; the active pocket/RNA-binding surface on the opposite side of RNase T is shown empty, and could presumably accommodate another substrate molecule in an analogous manner. Clashes in the docking models are mostly due to the long side chains of a few solvent-exposed basic residues (Arg101, Arg114, Lys139, and Arg140). These side chains are likely to adopt alternative conformations upon substrate binding.

E. coli tRNA genes encode the CCA ends, and 43% (37/86) of them have an additional A residue immediately following the CCA sequence. Due to the high flexibility of the α2 region on top of the DEDD cavity, it is difficult to predict with high confidence the specific interaction between RNase T and the terminal residues of the substrate based on docking. However, it is reasonable to speculate that the two terminal bases would stack between phenylalanine side chains, namely, between Phe77 and Phe29 and between Phe29 and Phe146, by analogy to the stacking of the terminal substrate base between Leu361 and Phe473 in the Klenow fragment (Beese and Steitz, 1991). Similar stacking has also been observed in structures of other DEDD exonucleases with substrates, such as the stacking of the terminal base between Ile34 and Phe115 in human PARN (Wu et al., 2005). In protein-RNA interactions, phenylalanine is typically disfavored in interactions with pyrimidine bases, especially cytidines (Jones et al., 2001). The "sandwiching" of terminal bases by phenylalanine side chains was speculated to account for RNase T discrimination of pyrimidine residues (Zuo and Deutscher, 2002c). However, a Phe29Tyr/Phe77Tyr double mutant did not significantly alter RNase T specificity (data not shown), suggesting a more complicated mechanism for its unusual base specificity.

Comparison to Other DEDD Exonucleases

E. coli has three DEDD family exoribonucleases—RNase T, oligoribonuclease (ORN), and RNase D (RND). RNase D is a monomeric enzyme of the DEDDy subfamily. It has two additional HRDC domains and forms a ring-like arrangement (Zuo et al., 2005). RNase T and oligoribonuclease are homodimeric DEDDh enzymes. Both RNase T and oligoribonuclease display strong RNase and DNase activity. ORN favors RNA oligonucleotides five nucleotides or shorter, with highest activity on dinucleotide substrates. In contrast, RNase T acts on longer substrates with essentially no activity on RNA dinucleotides. Although its specificity is not well defined, RNase D is highly active on tRNA-like substrates, namely tRNA precursors and denatured tRNAs. Corresponding to these differences in substrate specificity, we also observe differences in the architecture of these enzymes (Figure 6). RNT and ORN share very similar homodimeric arrangement, with major contribution of substrate binding from the complementing subunit. However, RNT has a large basic patch suitable for binding of longer substrates, while there is only a small basic patch on the ORN surface for favorable binding of short oligonucleotides. In favor of shorter substrates, ORN also has a unique elongated DEDD cavity long enough for three to four nucleotides (T.J. Fiedler, Y.Z., and A.M., unpublished data). Both RNT and ORN have deep DEDD cavities shaped by dimerization, whereas monomeric RND has a narrower DEDD cavity. RND also has an extended basic patch, on the HRDC domains, for potential substrate binding, though its ring structure may also play an important role in binding substrates (Zuo et al., 2005).

The use of basic patches for substrate binding appears to be a common feature of the three *E. coli* DEDD exoribonucleases. While the DEDD domain contributes the active site, another domain or subunit contributes to the basic patch. Unlike other DEDD exonucleases, RNT and ORN form homodimers. Interestingly, both RNT and ORN use equivalent regions for dimerization. For nonhomodimeric DEDD family members, this same interface region is involved in interdomain or intersubunit interactions.

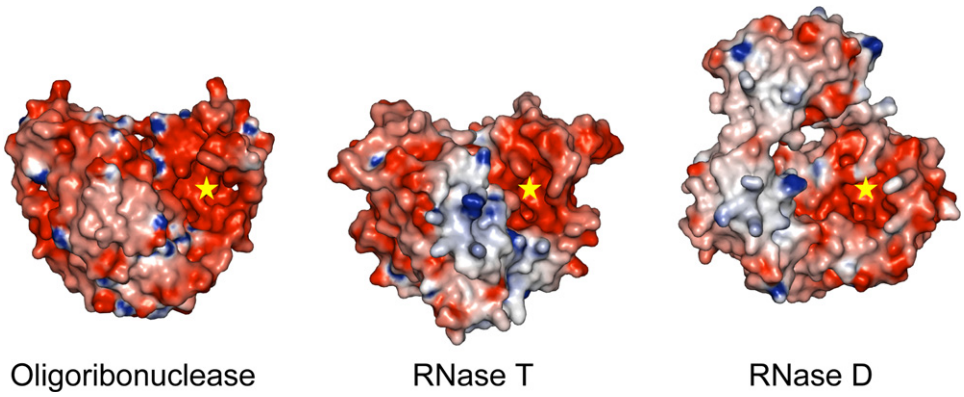

Figure 6. Comparison of the Structures of the Three DEDD Family Exoribonucleases from *E. coli*
Molecular surfaces colored by electrostatic potential are shown for these enzymes with one DEDD domain from each aligned in the same orientation. The active centers of these enzymes are highlighted (stars).

EXPERIMENTAL PROCEDURES

Cloning, Expression, Purification, and Crystallization

P. aeruginosa RNase T

The *P. aeruginosa* RNase T open reading frame was amplified by PCR from genomic DNA (American Type Culture Collection) as previously described (Zhang et al., 2001). The gene was cloned into the NdeI and BamHI sites of a modified pET15b expression vector, p11-toronto1 (Novagen). Modifications include a 6×His tag in a 22 amino acid N-terminal fusion peptide, with a TEV protease cleavage site, followed by a double stop codon downstream from the BamHI site. The resulting construct is an N-terminal 6×His tag separated from the gene by a TEV protease recognition site sequence (ENLYFQG). The modified pET15b vector containing the cloned *P. aeruginosa* RNT was then transformed into *E. coli* BL21(DE3) gold magic. Fresh transformants were inoculated into a 25 ml culture grown in a 250 ml flask with ampicillin, and then inoculated into 2 liters of Luria Broth (LB) (Invitrogen) in a custom-baffled 4 liter flask. The sample was induced at an optical density A_{600} of 0.6–0.8 with 0.4 mM isopropyl-1-thio-D-galactopyranoside (IPTG) after growth at 37°C and grown overnight at 15°C. The cells were harvested by centrifugation (10 min at 8,000 rpm; Beckman Coulter Avanti J-20 centrifuge). The cell pellet was resuspended in 40 ml binding buffer, supplemented with 1 mM each protease inhibitors phenylmethylsulfonyl fluoride (PMSF) and benzamidine, flash-frozen in liquid nitrogen, and stored at −70°C.

The purification procedure used buffers containing 50 mM HEPES (pH 7.5), 500 mM NaCl, 5% glycerol, and 5, 30, and 250 mM imidazole for the binding, wash, and elution buffers, respectively. The harvested cells were lysed by adding 0.5% Nonidet P-40 to the thawed sample before sonication. Fresh protease inhibitors were added before the sample was clarified by centrifugation (30 min at 17,000 rpm; Beckman Coulter Avanti J-25 centrifuge). The clarified lysate was passed by gravity through a DE52 column in series with an Ni^{2+} column. Contaminating proteins were removed by washing the Ni^{2+} column with 50 column volumes of wash buffer. The bound protein was removed with elution buffer as qualitatively determined by the Bradford assay (Bio-Rad protein assay) (Bradford, 1976). The sample was then supplemented with 0.5 mM EDTA and 0.5 mM dithiothreitol (DTT) (final concentration). The His tag was removed by cleavage with recombinant His-tagged TEV protease (60 μg TEV/mg recombinant protein). The cleavage step was done concurrently with dialysis in binding buffer without imidazole at 4°C overnight. The cut His tag and His-tagged TEV protease were removed from the purified recombinant protein by passage through a second Ni^{2+} column. The sample was prepared for crystallization screening by a second dialysis in 10 mM HEPES (pH 7.5), 500 mM NaCl, followed by concentration to 10 mg/ml using a BioMax concentrator (Millipore). Finally, any particulate matter was removed from the sample by passage through a 0.2 μm Ultrafree-MC centrifugal filtration device (Millipore) (Zhang et al., 2001).

The protein was crystallized at 20°C using the vapor diffusion method in sitting drops. A Cryschem plate (Hampton Research) was used in the crystallization setup. An initial hit was obtained with a Hampton Research Index screen, condition 82 (200 mM magnesium chloride hexahydrate, 25% w/v PEG3350, 100 mM Bis-Tris [pH 5.5]). After optimization, single, well-formed, diffraction-quality crystals were grown from a condition containing 25% w/v PEG3350, 200 mM magnesium chloride, 0.4% w/v NDSB256, and 300 mM Bis-Tris (pH 5.5).

E. coli RNase T

RNase T was initially overexpressed and purified using a pUT18-based overexpression system with the wild-type *rnt* gene cloned into the pUC18 vector (Zuo and Deutscher, 2002a). To achieve higher overexpression, the *E. coli* RNase T gene was cloned into the NcoI and BamHI sites of the pET15b expression vector (Novagen). The resulting pETT plasmid for wild-type RNase T production was confirmed by DNA sequencing. Plasmid pETT was then transformed into the *E. coli* BL21(DE3) strain for RNase T overexpression. RNase T was overexpressed by adding 1 mM IPTG (final concentration) to 2 liters of cells grown in LB with ampicillin to an A_{600} of ~1.0 at 37°C; the induction proceeded for about 2 hr. Cells were pelleted by centrifugation and then flash-frozen using liquid nitrogen and stored at −80°C.

RNase T was purified chromatographically using established procedures (Deutscher and Marlor, 1985; Li et al., 1996b) with some modifications. Briefly, the cell extract was applied on an Affi-Gel Blue column (Bio-Rad) followed by a hydroxyapatite column. RNase T was further purified and concentrated using a MonoQ anion exchange column (GE Healthcare). The RNase T-containing peak fractions were then applied on a Superdex S200 (GE Healthcare) gel filtration column equilibrated and eluted with a Tris buffer (20 mM Tris-Cl [pH 7.5], 250 mM NaCl, 1 mM DTT, and 10% glycerol). RNase T was then concentrated to 50 mg/ml. The concentrated protein was kept at −80°C after flash-freezing in liquid nitrogen. All centrifugation and chromatographic steps were carried out at 4°C. SeMet-RNT was produced from the same expression vector under conditions of methionine pathway inhibition as described previously (Fiedler et al., 2004). SeMet-RNT was purified in the same manner as the wild-type RNT.

E. coli RNase T protein crystallizes at room temperature in the presence of 2.3–2.9 M ammonium sulfate and various buffer conditions. The hanging-drop technique was used. RNase T crystals appear overnight and grow to more than 0.5 mm in size. These crystals are typically round shaped and diffract very poorly. The best diffracting crystals were grown from a condition containing 2.4 M ammonium sulfate and 100 mM 2-morpholinoethanesulfonic acid (MES) (pH 6.0).

Data Collection, Processing, and Structure Determination

P. aeruginosa RNase T

Prior to data collection, *P. aeruginosa* RNT crystals were transferred to a cryosolution prepared by addition of 9% glycerol, 9% ethylene glycol, 9% sucrose, and 0.2 M NaCl to the well solution, and frozen by plunging into liquid nitrogen. Data collection for *P. aeruginosa* RNT was performed on the 19ID beamline of the Structural Biology Center (Rosenbaum et al., 2006) at the Advanced Photon Source at 100K. Data collection, structure determination, and refinement statistics are summarized in Table 1. Data from Se-Met-labeled samples were processed with HKL-2000 (Otwinowski and Minor, 1997). Structures were solved using SAD data, and initial models were built with HKL-3000 (Minor et al., 2006) coupled with SHELXD (Schneider and Sheldrick, 2002), SHELXE (Sheldrick, 2002), CCP4 (Collaborative Computational Project, Number 4, 1994), MLPHARE (Otwinowski, 1991), DM (Cowtan, 1994), O (Jones et al., 1991), SOLVE (Terwilliger and Berendzen, 1999), and RESOLVE (Terwilliger, 2000). Initial models were refined with multiple runs of REFMAC5 (Murshudov et al., 1997) and manual model adjustments in Coot (Emsley and Cowtan, 2004). In the crystal structure of *P. aeruginosa* RNT, the first 18 residues (MSEDNFDDEFDGSLPSGP) and the last 4 residues (DDDD) could not be observed in the final electron-density map.

E. coli RNase T

Prior to data collection, *E. coli* RNT crystals were transferred to the reservoir solution and then transferred in steps to increase glycerol to about 20% for cryoprotection. Data collection was performed at 100K on the X12-C beamline, National Synchrotron Light Source, Brookhaven National Laboratory. Data were reduced using HKL-2000 (Otwinowski and Minor, 1997); phases were determined from a two-wavelength MAD experiment on SeMet-RNT. Twenty-four selenium sites (six per molecule) were found and refined in BnP (Xu et al., 2005). Albeit at 3.1 Å resolution, the initial map after solvent flattening (~70% solvent content) clearly displays ORN-like heart-shaped density for the RNase T dimer. The model was first roughly fitted with the homology model (Zuo and Deutscher, 2002b) and then manually built using O (Jones et al., 1991) and refined in CNS (Brunger et al., 1998). After several rounds of iterative model building and refinement, the final structure was refined at 3.1 Å with a simulated annealing procedure using CNS followed by REFMAC5 (Murshudov et al., 1997). In the crystal structure of *E. coli* RNT, two loop regions in molecule B (residues 27–36 and 65–84), as well as the first six residues and the last six residues in each monomer (last four residues of molecule B), were not built due to poor electron density.

Structure Validation

MOLPROBITY (Lovell et al., 2003) and PROCHECK (Laskowski et al., 1993) were used for structure validation. All model quality indicators were either within the normal range or better. Data collection, structure determination, and refinement statistics are summarized in Table 1. Molecular interface interactions were analyzed by using the Protein-Protein Interaction Server, available at http://www.biochem.ucl.ac.uk/bsm/PP/server (Jones and Thornton, 1996). All molecular figures were generated using PyMOL (DeLano, 2002), with surface potentials calculated using GRASP (Nicholls et al., 1991).

ACKNOWLEDGMENTS

We thank Professor Murray Deutscher for assistance and valuable discussions. We thank Anand Saxena at the X12-C beamline, National Synchrotron Light Source, Brookhaven National Laboratory, for assistance with data collection. NSLS financial support comes principally from the Offices of Biological and Environmental Research and of Basic Energy Sciences of the U.S. Department of Energy, and from the National Center for Research Resources of the National Institutes of Health. We thank all of the members of the Midwest Center of Structural Genomics and the Structural Biology Center at Argonne National Laboratory, especially Andrzej Joachimiak and Aled Edwards for discussions and assistance. Results shown in this report are derived from work performed at Argonne National Laboratory, Structural Biology Center at Advanced Photon Source. Argonne National Laboratory is operated by UChicago Argonne, LLC, for the U.S. Department of Energy, Office of Biological and Environmental Research, under contract DE-AC02-06CH11357. The work toward the *Escherichia coli* RNT structure was supported in part by National Institutes of Health grant GM69972 (A.M.). Y.Z. was supported in part by an American Heart Association Florida/Puerto Rico Affiliate Postdoctoral Fellowship (0525530B). The work toward the *Pseudomonas aeruginosa* RNT structure was supported by National Institutes of Health grant GM62414.

Received: November 30, 2006
Revised: February 12, 2007
Accepted: February 16, 2007
Published: April 17, 2007

REFERENCES

Beese, L.S., and Steitz, T.A. (1991). Structural basis for the 3′-5′ exonuclease activity of *Escherichia coli* DNA polymerase I: a two metal ion mechanism. EMBO J. *10*, 25–33.

Bradford, M.M. (1976). A rapid and sensitive method for the quantitation of microgram quantities of protein utilizing the principle of protein-dye binding. Anal. Biochem. *72*, 248–254.

Breyer, W.A., and Matthews, B.W. (2000). Structure of *Escherichia coli* exonuclease I suggests how processivity is achieved. Nat. Struct. Biol. *7*, 1125–1128.

Brunger, A.T., Adams, P.D., Clore, G.M., DeLano, W.L., Gros, P., Grosse-Kunstleve, R.W., Jiang, J.S., Kuszewski, J., Nilges, M., Pannu, N.S., et al. (1998). Crystallography & NMR system: a new software suite for macromolecular structure determination. Acta Crystallogr. D Biol. Crystallogr. *54*, 905–921.

CCP4 (Collaborative Computational Project, Number 4) (1994). The CCP4 suite: programs for protein crystallography. Acta Crystallogr. D Biol. Crystallogr. *50*, 760–763.

Cheng, Y., and Patel, D.J. (2004). Crystallographic structure of the nuclease domain of 3′hExo, a DEDDh family member, bound to rAMP. J. Mol. Biol. *343*, 305–312.

Cowtan, K. (1994). Joint CCP4 and ESF-EACBM Newsletter on Protein Crystallography *31*, 34–38.

DeLano, W.L. (2002). The PyMOL Molecular Graphics System (San Carlos, CA: DeLano Scientific).

Deutscher, M.P., and Marlor, C.W. (1985). Purification and characterization of *Escherichia coli* RNase T. J. Biol. Chem. *260*, 7067–7071.

Deutscher, M.P., Marlor, C.W., and Zaniewski, R. (1985). RNase T is responsible for the end-turnover of tRNA in *Escherichia coli*. Proc. Natl. Acad. Sci. USA *82*, 6427–6430.

Emsley, P., and Cowtan, K. (2004). Coot: model-building tools for molecular graphics. Acta Crystallogr. D Biol. Crystallogr. *60*, 2126–2132.

Ezraty, B., Dahlgren, B., and Deutscher, M.P. (2005). The RNase Z homologue encoded by *Escherichia coli* elaC gene is RNase BN. J. Biol. Chem. *280*, 16542–16545.

Fiedler, T.J., Vincent, H.A., Zuo, Y., Gavrialov, O., and Malhotra, A. (2004). Purification and crystallization of *Escherichia coli* oligoribonuclease. Acta Crystallogr. D Biol. Crystallogr. *60*, 736–739.

Gilliland, G.L., Teplyakov, A., Obmolova, G., Tordova, M., Thanki, N., Ladner, J., Herzberg, O., Lim, K., Zhang, H., Huang, K., et al. (2002). Assisting functional assignment for hypothetical *Heamophilus influenzae* gene products through structural genomics. Curr. Drug Targets Infect. Disord. *2*, 339–353.

Hamdan, S., Carr, P.D., Brown, S.E., Ollis, D.L., and Dixon, N.E. (2002). Structural basis for proofreading during replication of the *Escherichia coli* chromosome. Structure *10*, 535–546.

Holm, L., and Sander, C. (1996). Mapping the protein universe. Science *273*, 595–603.

Hopfner, K.P., Eichinger, A., Engh, R.A., Laue, F., Ankenbauer, W., Huber, R., and Angerer, B. (1999). Crystal structure of a thermostable type B DNA polymerase from *Thermococcus gorgonarius*. Proc. Natl. Acad. Sci. USA *96*, 3600–3605.

Horio, T., Murai, M., Inoue, T., Hamasaki, T., Tanaka, T., and Ohgi, T. (2004). Crystal structure of human ISG20, an interferon-induced antiviral ribonuclease. FEBS Lett. *577*, 111–116.

Jones, S., and Thornton, J.M. (1996). Principles of protein-protein interactions. Proc. Natl. Acad. Sci. USA *93*, 13–20.

Jones, T.A., Zou, J.Y., Cowan, S.W., and Kjeldgaard, M. (1991). Improved methods for building protein models in electron density maps and the location of errors in these models. Acta Crystallogr. A *47*, 110–119.

Jones, S., Daley, D.T., Luscombe, N.M., Berman, H.M., and Thornton, J.M. (2001). Protein-RNA interactions: a structural analysis. Nucleic Acids Res. *29*, 943–954.

Kelly, K.O., and Deutscher, M.P. (1992). The presence of only one of five exoribonucleases is sufficient to support the growth of *Escherichia coli*. J. Bacteriol. *174*, 6682–6684.

Koonin, E.V., and Deutscher, M.P. (1993). RNase T shares conserved sequence motifs with DNA proofreading exonucleases. Nucleic Acids Res. *21*, 2521–2522.

Laskowski, R.A., MacArthur, M.V., Moss, D.S., and Thornton, J.M. (1993). PROCHECK: a program to check the stereochemical quality of protein structures. J. Appl. Cryst. *26*, 283–291.

Li, Z., and Deutscher, M.P. (1995). The tRNA processing enzyme RNase T is essential for maturation of 5S RNA. Proc. Natl. Acad. Sci. USA *92*, 6883–6886.

Li, Z., and Deutscher, M.P. (1996). Maturation pathways for *E. coli* tRNA precursors: a random multienzyme process in vivo. Cell *86*, 503–512.

Li, Z., Zhan, L., and Deutscher, M.P. (1996a). *Escherichia coli* RNase T functions in vivo as a dimer dependent on cysteine 168. J. Biol. Chem. *271*, 1133–1137.

Li, Z., Zhan, L., and Deutscher, M.P. (1996b). The role of individual cysteine residues in the activity of *Escherichia coli* RNase T. J. Biol. Chem. *271*, 1127–1132.

Li, Z., Pandit, S., and Deutscher, M.P. (1998). 3′ exoribonucleolytic trimming is a common feature of the maturation of small, stable RNAs in *Escherichia coli*. Proc. Natl. Acad. Sci. USA *95*, 2856–2861.

Li, Z., Pandit, S., and Deutscher, M.P. (1999). Maturation of 23S ribosomal RNA requires the exoribonuclease RNase T. RNA *5*, 139–146.

Lovell, S.C., Davis, I.W., Arendall, W.B., III, de Bakker, P.I., Word, J.M., Prisant, M.G., Richardson, J.S., and Richardson, D.C. (2003). Structure validation by Cα geometry: ϕ,ψ and Cβ deviation. Proteins *50*, 437–450.

Minor, W., Cymborowski, M., Otwinowski, Z., and Chruszcz, M. (2006). HKL-3000: the integration of data reduction and structure solution—from diffraction images to an initial model in minutes. Acta Crystallogr. D Biol. Crystallogr. *62*, 859–866.

Murshudov, G.N., Vagin, A.A., and Dodson, E.J. (1997). Refinement of macromolecular structures by the maximum-likelihood method. Acta Crystallogr. D Biol. Crystallogr. *53*, 240–255.

Nicholls, A., Sharp, K.A., and Honig, B. (1991). Protein folding and association: insights from the interfacial and thermodynamic properties of hydrocarbons. Proteins *11*, 281–296.

Notredame, C., Higgins, D.G., and Heringa, J. (2000). T-Coffee: a novel method for fast and accurate multiple sequence alignment. J. Mol. Biol. *302*, 205–217.

Otwinowski, Z. (1991). Proceedings of the CCP4 study weekend. In Isomorphous Replacement and Anomalous Scattering, W. Wolf, P.R. Evans, and A.G.W. Leslie, eds. (Warrington, UK: Daresbury Laboratory), pp. 80–86.

Otwinowski, Z., and Minor, W. (1997). Processing of X-ray diffraction data collected in oscillation mode. Methods Enzymol. *276*, 307–326.

Rosenbaum, G., Alkire, R.W., Evans, G., Rotella, F.J., Lazarski, K., Zhang, R.G., Ginell, S.L., Duke, N., Naday, I., Lazarz, J., et al. (2006). The Structural Biology Center 19ID undulator beamline: facility specifications and protein crystallographic results. J. Synchrotron Radiat. *13*, 30–45.

Schneider, T.R., and Sheldrick, G.M. (2002). Substructure solution with SHELXD. Acta Crystallogr. D Biol. Crystallogr. *58*, 1772–1779.

Sheldrick, G.M. (2002). Macromolecular phasing with SHELXE. Z. Kristallogr. *217*, 644–650.

Steitz, T.A., and Steitz, J.A. (1993). A general two-metal-ion mechanism for catalytic RNA. Proc. Natl. Acad. Sci. USA *90*, 6498–6502.

Terwilliger, T.C. (2000). Maximum-likelihood density modification. Acta Crystallogr. D Biol. Crystallogr. *56*, 965–972.

Terwilliger, T.C., and Berendzen, J. (1999). Automated MAD and MIR structure solution. Acta Crystallogr. D Biol. Crystallogr. *55*, 849–861.

Thore, S., Mauxion, F., Seraphin, B., and Suck, D. (2003). X-ray structure and activity of the yeast Pop2 protein: a nuclease subunit of the mRNA deadenylase complex. EMBO Rep. *4*, 1150–1155.

Viswanathan, M., Dower, K.W., and Lovett, S.T. (1998). Identification of a potent DNase activity associated with RNase T of *Escherichia coli*. J. Biol. Chem. *273*, 35126–35131.

Wu, M., Reuter, M., Lilie, H., Liu, Y., Wahle, E., and Song, H. (2005). Structural insight into poly(A) binding and catalytic mechanism of human PARN. EMBO J. *24*, 4082–4093.

Xu, H., Weeks, C.M., and Hauptman, H.A. (2005). Optimizing statistical Shake-and-Bake for Se-atom substructure determination. Acta Crystallogr. D Biol. Crystallogr. *61*, 976–981.

Zhang, R.G., Skarina, T., Katz, J.E., Beasley, S., Khachatryan, A., Vyas, S., Arrowsmith, C.H., Clarke, S., Edwards, A., Joachimiak, A., and Savchenko, A. (2001). Structure of *Thermotoga maritima* stationary phase survival protein SurE: a novel acid phosphatase. Structure *9*, 1095–1106.

Zuo, Y., and Deutscher, M.P. (1999). The DNase activity of RNase T and its application to DNA cloning. Nucleic Acids Res. *27*, 4077–4082.

Zuo, Y., and Deutscher, M.P. (2001). Exoribonuclease superfamilies: structural analysis and phylogenetic distribution. Nucleic Acids Res. *29*, 1017–1026.

Zuo, Y., and Deutscher, M.P. (2002a). Mechanism of action of RNase T. I. Identification of residues required for catalysis, substrate binding, and dimerization. J. Biol. Chem. *277*, 50155–50159.

Zuo, Y., and Deutscher, M.P. (2002b). Mechanism of action of RNase T. II. A structural and functional model of the enzyme. J. Biol. Chem. *277*, 50160–50164.

Zuo, Y., and Deutscher, M.P. (2002c). The physiological role of RNase T can be explained by its unusual substrate specificity. J. Biol. Chem. *277*, 29654–29661.

Zuo, Y., Wang, Y., and Malhotra, A. (2005). Crystal structure of *Escherichia coli* RNase D, an exoribonuclease involved in structured RNA processing. Structure *13*, 973–984.

Accession Numbers

Atomic coordinates and experimental structure factors have been deposited with the RCSB Protein Data Bank under ID code 2F96 for *Pseudomonas aeruginosa* RNase T and ID code 2IS3 for *Escherichia coli* RNase T.

